

# A 32 by 32 Electroplated Metallic Micromirror Array

Jeong-Bong Lee

**Abstract**—This paper presents the design, fabrication and characterization of a 32 by 32 electroplated micromirror array on a glass, a low cost substrate. Approaches taken in this work for the fabrication of micromachined mirror arrays include a line addressing scheme, a seamless array design for high fill factor, planarization techniques of polymeric interlayers, a high yield methodology for the removal of sacrificial polymeric interlayers, and low temperature and chemically safe fabrication techniques. The micromirror is fabricated by aluminum and the size of a single micromirror is  $200\ \mu\text{m} \times 200\ \mu\text{m}$ . Static deflection test of the micromirror has been carried out and pull-in voltage of 44 V and releasing voltage of 30V was found.

**Index Terms**—micromirror array, finite element modeling, electrostatic, electroplating, sacrificial layer

## I. INTRODUCTION

The massive growth of the electronic industry has led to the development of electronic displays which serve as key user interfaces. Flat panel displays (FPD) were originally driven by a vision of a large, thin television screen to hang on the wall. With the advent of laptop and

notebook personal computers, flat panel displays began to be commercialized in the 1980's. FPDs can be divided into two main categories: emissive and nonemissive displays. Emissive FPDs include electroluminescence (EL) displays [1], plasma display panels (PDP) [2], field emission displays (FED) [3], and vacuum fluorescent displays (VFD) [4]. Nonemissive FPDs include liquid crystal displays (LCD) [5], digital micromirror device (DMD<sup>TM</sup>) [6] based displays, and grating light valve (GLV<sup>TM</sup>) [7] based displays.

A 32 by 32 micromirror array reported in this work is similar to the Texas Instruments' DMD [6], but has several different approaches with the goal of enabling low cost manufacturing. The micromirror arrays have been built on low cost substrates, such as glass, instead of relatively expensive CMOS-processed underlying circuitry. Such an approach allows the realization of relatively low cost, passive micromirror array elements. Approaches taken in this work for the fabrication of micromachined mirror arrays include a line addressing scheme [8], a seamless array design for high fill factor, planarization techniques of polymeric interlayers [9], a high yield methodology for the removal of sacrificial polymeric interlayers, and low temperature and chemically safe fabrication techniques.

## II. DESIGN

The micromirror is nearly square-shaped and is suspended at its center by thin and narrow hinges which are supported at their ends by electroplated nickel posts. The fill factor is defined as the area of reflecting light in a mirror pixel divided by the total area of a mirror pixel. A higher fill factor results in higher perceived resolution, yielding more natural images. Therefore, a seamless design is desirable for display application. The size of the micromirror is  $190\ \mu\text{m}$  on a side, the width of the

---

Manuscript received November 16, 2002; revised December 12, 2002.  
Erik Jonsson School of Engineering and Computer Science,  
University of Texas at Dallas 2601 N. Floyd Rd., Richardson, Texas  
70803-0688

E-mail: jblee@utdallas.edu

Tel : (972) 883-2893

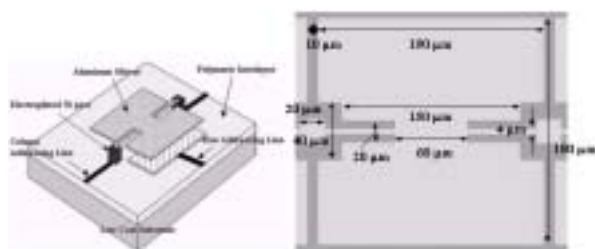


Fig. 1. A schematic drawing of a micromachined mirror.

hinge is 4 μm, and the pixel pitch size is 200 μm. The fill factor for this micromirror is 83.75 % (33,500 μm<sup>2</sup> / 40,000 μm<sup>2</sup>). The thickness of the organic sacrificial layer (i.e., the air gap for micromirror actuation) ranges from 18 μm to 24 μm, resulting in deflection angle ranges from 10.7° to 14.2°.

### III. FINITE ELEMENT MODELING FOR RESONANT FREQUENCIES

Finite element modeling (FEM) of the micromirror was performed using the finite element modeling package ANSYS™ to calculate resonant frequencies and mode shapes. The material parameters used in the FEM are bulk materials properties of aluminum and it is showed in Table 1. The element type used has eight nodes with six degrees of freedom (DOF) at each node: displacements in nodal x, y, and z directions and rotations about nodal x, y, and z-axes. Since the hinge is

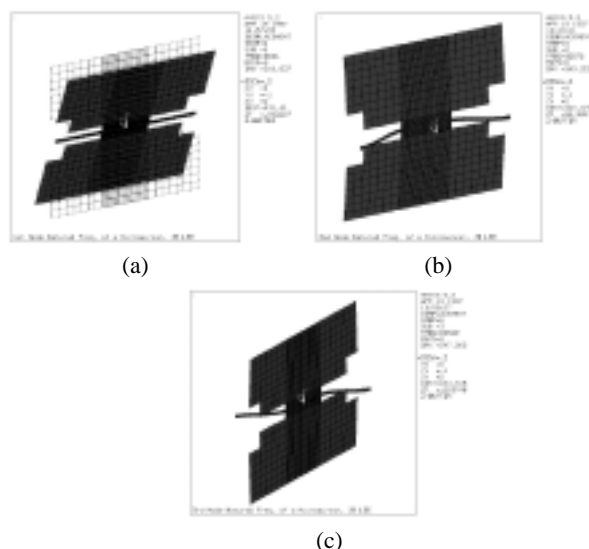


Fig. 2. Resonant mode shapes of the micromirror: (a) fundamental mode; (b) second mode; (s) third mode.

the area of interest for torsional behavior of the micromirror, hinges and adjacent areas were densely meshed while most of the plate was coarsely meshed.

Figure 2 show the first three mode shapes of the micromirror. The fundamental mode resonant frequency is 6.5 kHz which is the determining factor for the switching speed of the micromirror. Since this micromirror array uses a line addressing scheme, the minimum time field for one frame is 4.92 ms (153.8 μs \* 32 = 4.92 ms). If the micromirror array works as a black & white display (no gray scale), then the maximum frame rate would be as high as 203.3 Hz (1/4.92 ms).

### IV. FABRICATION

A brief fabrication procedure is shown in Figure 3. Fabrication of micromirror arrays started with 3 inch by 2 inch glass substrates. Evaporated Ti/Au (thickness of 300 / 4,000 Å) row addressing lines were patterned using the liftoff process. A benzocyclobutene (BCB, Dow) layer was spin-coated to planarize the patterned metallic lines. A silicon dioxide (SiO<sub>2</sub>) passivation layer was deposited using plasma enhanced chemical vapor deposition (PECVD) to protect the BCB layer during the very last step of dry etching for bonding pad opening. Evaporated Ti/Au (300 / 4,000 Å) column addressing lines (also serving as an electroplating seed layer for posts) were patterned using the liftoff process. Two different organic interlayers, both single and double coats of PI 2611 (DuPont), were spin coated as polymeric sacrificial layers. In the case of a single coat of PI 2611, the coated layer was soft baked at 150 °C for 30 minutes. The thickness of the soft-baked single coat of PI 2611 layer was approximately 18 μm. In the case of a double coat of PI 2611, samples were soft baked after each spin at 120 °C for 20 minutes and hard baked at 300 °C for one hour in nitrogen ambient after the second coat. The double-coated PI 2611 thickness was approximately 24 μm. A 1,000 Å aluminum hard mask was prepared for via cutting by the liftoff process. Reactive ion etching (incident power of 300 W, pressure of 300 mTorr or less, oxygen gas flow rate of 50 sccm) was used to define 10 μm by 10 μm square via holes. Etch rate was about 0.25 μm/min. for hard cured PI 2611, and 0.6 μm/min. for soft cured PI 2611. After via cut, the

aluminum hard mask was removed by diluted hydrofluoric acid (HF) which was followed by nickel (Ni) electroplating. After the Ni electroplating, the surface of the polyimide electroplating mold and plated Ni had roughness of about less than 1  $\mu\text{m}$ . A 7,000  $\text{\AA}$  aluminum layer was then deposited using DC sputtering and patterned to form hinge and micromirror plate structures. Finally, the organic sacrificial layer was etched away by an isotropic dry etch using a barrel plasma etcher. Figure 4 shows SEM photomicrographs of a side view of the corner of the completely released 32 by 32 micromirror array, a close-up view of the electroplated nickel post and the Ti/Au seed layer, and top views of a part of micromirror array and a single

micromirror. The organic interlayer was safely and completely removed and left overhanging micromirror array structures. The gap between micromirror plates and the planarization BCB layer is 18  $\mu\text{m}$ , which allows 10.8° angular deflection.

### V. MICROMIRROR ACTUATION AND MECHANICAL CHARACTERIZATION

The completely released micromirror array was placed on an optical microscope and the gap between the micromirror and planarized BCB/SiO<sub>2</sub> layer was measured to be 18  $\mu\text{m}$ . The deflection of the tip of the micromirror was measured by focusing on the tip of the micromirror using a Nikon MM-11 Measurescope and measuring the deflection of the microscope head necessary to keep the deflecting tip in focus. The displacement characteristic (deflection versus applied voltage) is shown in Figure 5 (a). The measured pull-in voltage ( $V_p$ ) is 44 V, and the releasing voltage ( $V_r$ ) is approximately 30V.



Fig. 3. Fabrication procedures for micromachined mirror arrays on low cost substrates.

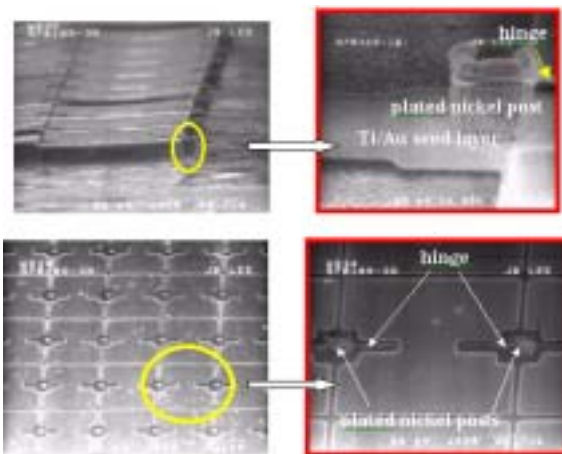
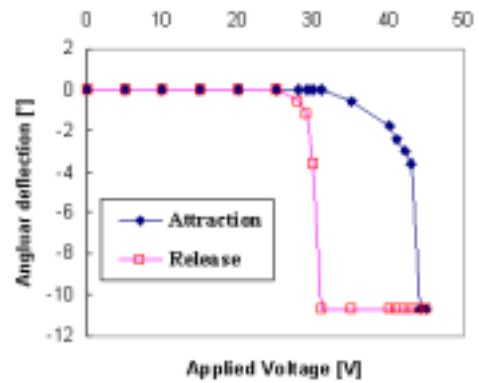
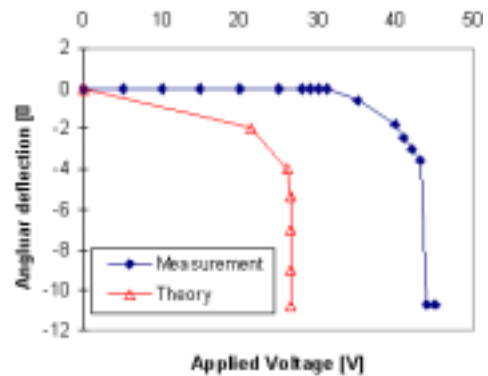


Fig. 4. SEM photomicrographs of completely released 32 by 32 micromirror array.



(a)



(b)

Fig. 5. Displacement characteristic of the micromirror.

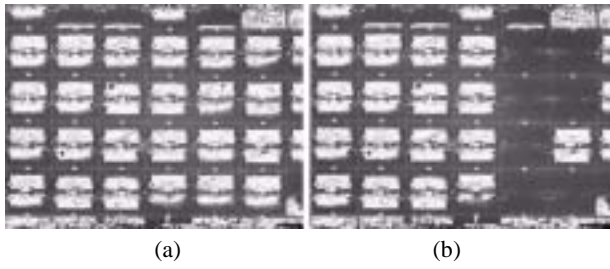


**Fig. 6.** Optical micrographs of a part of micromirror array: (a) undeflected; (b) several pixels at right of array energized and deflected.

The fabricated 32 by 32 micromirror array was placed on a probe station (Signatone S-1160A-6N) and directly connected to the output of a power supply (Hewlett Packard 6622A DC Power Supply) through probes (Signatone S-725). The device was observed using an optical microscope with video camera, connected to a display monitor and a video cassette recorder (VCR). Individual and a part of array micromirror actuation were observed and recorded using a VCR. Figure 6 shows optical micrographs of a part of the micromirror array, undeflected (a), and several pixels at right side of the array energized and deflected (b), respectively.

### VI. THEORETICAL MECHANICAL MODELING

Theoretical modeling for the static deflection of the micromirror was performed with several assumptions and those results are compared with the measurement results. Figure 7 shows the schematic diagram of a cross section of a micromirror used for the theoretical modeling. When an external voltage is applied between the grounded micromirror and the address electrode, a potential energy  $W$  is stored in the system. The electrostatic force which acts normal to the substrate is complex since there is a fringing effect, and the direction of the electrostatic force changes as the micromirror rotates. Simple theoretical models, however, may be established with following assumptions: (1) the hinge is straight, of uniform rectangular cross section, and of homogeneous isotropic material; (2) the hinge is loaded only by equal and opposite twisting couples, which are applied at its ends in planes normal to its axis; (3) the hinge is not stressed beyond the elastic limit; (4) the fringing electric field is negligible. In reality, the fringing

**Table 1.** Material properties and geometrical parameters used in theoretical modeling.

Material Properties		Geometrical Parameters	
Young's modulus of Al	70 GPa	$Z_0$	18 $\mu\text{m}$
Poisson ratio of Al	0.33	$Z_1$	2.5 $\mu\text{m}$
Shear modulus of Al	26.3 GPa	$Z_2$	0.5 $\mu\text{m}$
Density of Al	2710 $\text{kg/m}^3$	$t$	0.7 $\mu\text{m}$
		$w$	4 $\mu\text{m}$
Relative permittivity of BCB	2.7	$a$	190 $\mu\text{m}$
Relative permittivity of $\text{SiO}_2$	3.9	$b$	190 $\mu\text{m}$
		$L$	60 $\mu\text{m}$

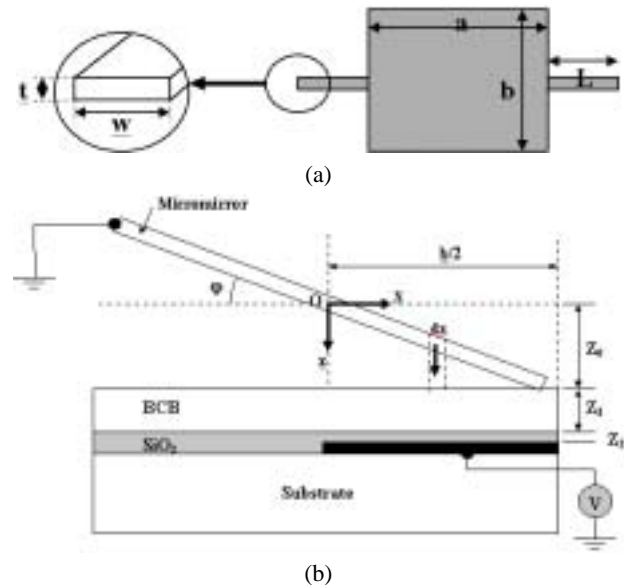


**Fig. 7.** A schematic diagram of a single micromirror: (a) top view and a close-up view of the hinge; (b) cross section of a micromirror.

effect should not be neglected, but this assumption was made for this simple theoretical model. Figure 6 and Table 1 show the material properties and geometrical parameters used in the theoretical modeling.

The mechanical torque  $T_m$  is defined as follows:

$$T_m = k\phi = \frac{GI_p}{L} \phi \tag{1}$$

where  $k$  is the torsional spring constant,  $\phi$  is the deflected angle in radians,  $G$  is the shear modulus of elasticity,  $I_p$  is the polar moment of inertia, and  $L$  is the length of the hinge. The shear modulus of elasticity  $G$  is

defined as follows:

$$G = \frac{E}{2(1+\nu)}, \quad (2)$$

where  $E$  is the Young's modulus, and  $\nu$  is the Poisson ratio.

For the beam with aspect ratio (thickness/width) lower than 1 (1 = square cross section), theoretical expression for the polar moment of inertia ( $I_p$ ) is given [10] as follows:

$$I_p = \left(\frac{w}{2}\right)\left(\frac{t}{2}\right)^3 \left[ \frac{16}{3} - 3.36 \left(\frac{t}{w}\right) \left(1 - \frac{t^4}{12w^4}\right) \right] \quad (3)$$

At the maximum deflection ( $\varphi=10.8^\circ=0.1885$  rad), the mechanical torque  $T_m$  turned out to be  $3.3622 \times 10^{-11}$  [N-m] based on equation (3). The electrostatic torque  $T_{el}$  can be represented as the following expression:

$$T_{el} = \frac{\partial W_{el}}{\partial \varphi} = \frac{V^2}{2} \frac{\partial}{\partial \varphi} \left( \int_0^{b/2} dC \right), \quad (4)$$

where  $W_{el}$  is the electrostatic energy stored in the system,  $V$  is the applied voltage,  $C$  is the capacitance of the system. Since the rotation angle for this micromirror is small (between  $0^\circ$  and  $10.8^\circ$ ), the tangent of  $\varphi$  could be assumed equal to  $\varphi$ . The maximum error due to this assumption is 1.2 %. The analytical solution for the electrostatic torque  $T_{el}$  is calculated using Mathematica™. The Taylor expansion of the analytical solution about  $\varphi = 0$  is:

$$T_{el} = \frac{ab^2 \varepsilon_{r1}^2 \varepsilon_{r2}^2 \varepsilon_0 V^2}{16(\varepsilon_{r1} \varepsilon_{r2} z_0 + \varepsilon_{r2} z_1 + \varepsilon_{r1} z_2)^2} + \frac{ab^3 \varepsilon_{r1}^3 \varepsilon_{r2}^3 \varepsilon_0 V^2}{24(\varepsilon_{r1} \varepsilon_{r2} z_0 + \varepsilon_{r2} z_1 + \varepsilon_{r1} z_2)^3} \varphi + \frac{3ab^4 \varepsilon_{r1}^4 \varepsilon_{r2}^4 \varepsilon_0 V^2}{128(\varepsilon_{r1} \varepsilon_{r2} z_0 + \varepsilon_{r2} z_1 + \varepsilon_{r1} z_2)^4} \varphi^2 + \frac{ab^5 \varepsilon_{r1}^5 \varepsilon_{r2}^5 \varepsilon_0 V^2}{80(\varepsilon_{r1} \varepsilon_{r2} z_0 + \varepsilon_{r2} z_1 + \varepsilon_{r1} z_2)^5} \varphi^3 + [\dots] \varphi^4 \quad (5)$$

The first term is same as the parallel plate capacitor

case. Higher order terms correct for the fact that the capacitance and torque change nonlinearly as the micromirror rotates. Figure 5 (b) shows the theoretical model for the attraction cycle of the micromirror compared with the measurement data. The discrepancy is within 39 %.

The discrepancy between the measurement data and the theoretical model for the attraction cycle of the static deflection characteristics of the micromirror could be due to a combination of several causes. First, and most importantly, the theoretical model does not include the residual stress effect. If the residual stress is compressive, microstructures are buckled and this stress state can be noticed by a visual inspection. The tensile stress is less noticeable, but its effect on torsional deflection behavior can be large. It is known that the residual stress effect becomes larger as the aspect ratio (thickness/width) of the hinge becomes smaller [11]. In this work, the aspect ratio is approximately 0.175 ( $0.7 \mu\text{m}/4 \mu\text{m}$ ), so the tensile residual stress of 0.79 GPa (which is approximately 1 % of the Young's modulus of Al) can increase the required voltage for pull-in. The second important cause could be measurement errors in the geometrical parameters of the hinge of the micromirror. If there is a 10 % measurement error in the thickness of the hinge, then the polar moment of inertia changes 33.1 %, and subsequently the required voltage changes 15.4 %. A combination of these two causes and other minor causes may make the 39 % discrepancy between the measurement data and the theoretical model.

## VII. OPTICAL CHARACTERIZATION

The optical reflectivity and the switching characteristics of the micromirror were measured using a helium-neon (He-Ne) laser (wavelength of 632.8 nm, SpectraPhysics Model 127). The diameter of the beam spot size of the He-Ne laser used in this research is approximately 3 mm. Since the beam spot size of the laser is much larger than that of the micromirror ( $190 \mu\text{m}$  on a side), the reflectivity test cannot be done by steering the beam onto an individual micromirror. Therefore, a sample was prepared for the measurement of the reflectivity of the surface of the micromirror. The sample was sputter deposited aluminum (thickness of  $7,000 \text{ \AA}$ ,

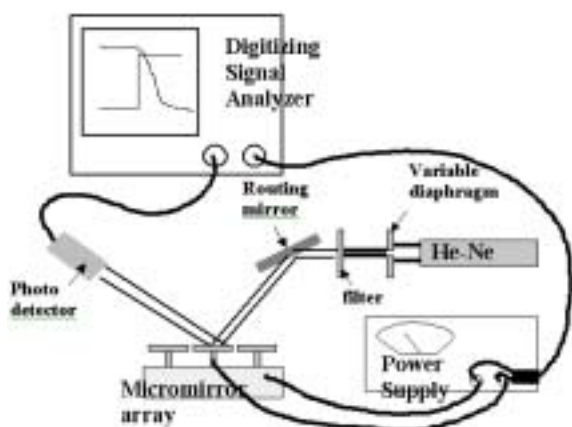


**Fig. 8.** A schematic diagram of the experimental setup for the optical characterization.

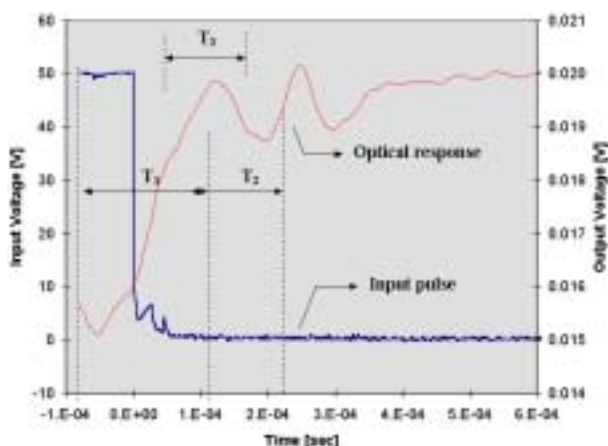


**Fig. 9.** Optical response of the micromirror when it is abruptly turned off.

the same condition used in depositing micromirror array) on a 3 inch by 2 inch glass substrate. The reflectivity of the surface of the sputter deposited Al was measured using a LiConix Laser Power Meter 45PM and an Ophir Optronix Nova Display. The measured incident power using the LiConix was 34 mW and the reflected power was 28.4 mW, yielding a reflectivity of 83.5 %. The incident power measured using the Ophir was 29 mW and the reflected power was 25 mW, yielding a reflectivity of 86.2 %. This reflectivity value agrees well with literature values of 83 % reflectivity for Al [12].

The switching characteristic of the micromirror was measured using an experimental setup shown in Figure 8. Since the diameter of the laser beam spot is large (about 3 mm), a variable diaphragm was used to make a smaller beam spot size (1mm) in an attempt to make as small a beam spot as possible. A routing mirror steers the laser

beam into the surface of the torsional micromirror, and the reflected laser beam from the surface of the micromirror was measured by a high speed silicon photo detector (Thorlabs Inc., DET 100, rise time 20 nsec.). The detected signal and the applied signal were connected to a Tektronix DSA 602 Digitizing Signal Analyzer through an 11A32 Two Channel Amplifier (bandwidth of 400 MHz). While the micromirror is turned off (applied voltage of 0 V), the reflected laser is directly incident on the photo detector. Once the micromirror is turned on, the micromirror deflects 10.8°, and the reflected laser beam is moved out of the detecting area of the photo detector.

When the micromirror is abruptly turned on (from 0 V to 44V), the micromirror deflects 10.8°. No oscillations of the optical response were observed, presumably since the micromirror hit the surface of the BCB/SiO<sub>2</sub> interlayer. The rise time is approximately 30 μs and the time to reach to the first peak is approximately 78 μs. The delay time for the optical response is measured as approximately 8 μs. When the micromirror is abruptly turned off (from 44 V to 0 V), the micromirror moves back to its original flat position (angular deflection of 0°). As shown in Figure 9, when the micromirror moves back, oscillation of the optical response is observed. The time  $t_1$  is approximately 180 μs,  $t_2$  approximately 120 μs, and  $t_3$  approximately 140 μs, respectively.

## CONCLUSIONS

A 32 by 32 micromachined mirror array is designed, fabricated, and characterized for generic optical applications. Finite element modeling of resonant frequencies of micromirror was carried out and the fundamental resonant frequency for the 190 μm aluminum micromirror was found to be 6.5 kHz. The micromirror array was fabricated by polymeric/metallic multilayer processing techniques. It has a large deflection angle (~ 10.8°) and the pull-in voltage was measured as 44 V. Theoretical mechanical modeling was carried out and the result of the modeling and the measurement were compared. Optical characterization was also carried out to analyze the behaviors of the micromirror in response to input electrical signal. The

micromirror array can be fabricated on low cost substrates and it can be used for a wide variety of optical applications.

### ACKNOWLEDGEMENTS

Material donations from Dow Chemical are greatly appreciated. Microfabrication was carried out at the Georgia Tech Microelectronics Research Center. The support of the staff of the Pettit Microelectronics Research Center at Georgia Tech is acknowledged. Technical discussions with Dr. Mark G. Allen of Georgia Tech are greatly appreciated. The optical characterization was carried out at the Georgia Tech Research Institute (GTRI). The support of the staff of the GTRI and Dr. Won Park are greatly appreciated. The secretarial support of the staff of the Department of Electrical Engineering at the University of Texas at Dallas is acknowledged.

### REFERENCES

- [1] C. N. King, "Electroluminescent displays," *Journal of the Society for Information Display*, vol. 4, no. 1, pp. 1-8, 1996.
- [2] H. Uchiike and T. Hirakawa, "Color plasma displays," *Proceedings of the IEEE*, vol. 90, no. 4, pp. 533-539, 2002.
- [3] A. A. Talin, K. A. Dean, and J. E. Jaskie, "Field emission displays: A critical review," *Solid State Electronics*, vol. 45, no. 6, pp. 963-976, 2001.
- [4] Y. Yoshida, A. Ishizuka, and H. Makishima, "Present and future of vacuum fluorescent display and field emission display," *Materials Chemistry and Physics*, vol. 40, no. 4, pp. 267-272, 1995.
- [5] K. Tarumi, M. Heckmeier, and M. Klasen-Memmer, "Advanced liquid-crystal materials for TFT monitor and TV applications," *Journal of the Society for Information Display*, vol. 10, no. 2, pp. 127-132, 2002.
- [6] L. J. Hornbeck, "The DMD™ projection display chip: a MEMS-based technology," *MRS Bulletin*, vol. 26, no. 4, pp. 325-327, 2001.
- [7] D. T. Amm and R. W. Corrigan, "Optical performance of the grating light valve technology," in *Proceedings of SPIE, Projection Displays V*, SPIE vol. 3634, pp. 71-78, 1999.
- [8] V. P. Jaecklin, C. Linder, N. F. De Rooij, J. M. Moret, and R. Vuilleumier, "Line-addressible torsional micro-

mirrors for light modulator arrays," *Sensors and Actuators A*, vol. 41-42, pp. 324-329, 1994.

- [9] Jeong B. Lee, J. English, C. H. Ahn, and M. G. Allen, "Planarization Techniques for Vertically Integrated Metallic MEMS on Silicon Foundry Circuits," *Journal of Micromechanics and Microengineering*, vol. 7, no. 2, pp. 44-54, 1997.
- [10] Roark, "Formulas for stress and strain," *McGraw-Hill*, p. 349.
- [11] J. A. Connally, "Torsion of a thin rectangular beam with axial prestress and ends constrained from warping," *M.S. Thesis*, p. 30, Massachusetts Institute of technology, Cambridge, MA, 1986.
- [12] V. P. Jaecklin, C. Linder, J. Brugger, N. F. De Rooij, J. M. Moret, and R. Vuilleumier, "Mechanical and optical properties of surface micromachined torsional mirrors in silicon, polysilicon and aluminum," *Sensors and Actuators A*, vol. 43, pp. 269-275, 1994.



**Jeong-Bong Lee** received the B.S. degree in electronics engineering from Hanyang University, Seoul, Korea, in 1986 and the M.S. and the Ph.D. degrees in electrical engineering from Georgia Institute of Technology, Atlanta, Georgia, in 1993 and 1997, respectively. He had worked for Georgia Tech as a research engineer upon his graduation. In January 1999, he joined Louisiana State University, Baton Rouge, Louisiana as an assistant professor. Since May 2001, he has been with the University of Texas at Dallas as an assistant professor in the Department of Electrical Engineering. His current research interests in the Department of Electrical Engineering. His current research interests are developments of passive components for RF/microwave MEMS, development of packaging technique for system-on-a-chip (SoC), nano-photonics devices, micro/nano assemblers for MEMS and NEMS, and injection molding-based BioMEMS. He is a recipient of the National Science Foundation's Faculty Early Career Development Award.